Spectrochimica Acta Part B: Atomic Spectroscopy 193 (2022) 106430

Contents lists available at ScienceDirect

Spectrochimica Acta Part B: Atomic Spectroscopy

journal homepage: www.elsevier.com/locate/sab

Laser induced breakdown spectroscopy with annular plasmas in vacuo: Stagnation and limits of detection☆

B. Delaney [a,b], P. Hayden [a], T.J. Kelly [c,*], E.T. Kennedy [b], J.T. Costello [b]

[a] School of Physics, Science Centre North, University College Dublin, Belfield, Dublin 4, Ireland
[b] School of Physical Sciences, Dublin City University, Glasnevin, Dublin 9, Ireland
[c] Department of Computer Science and Applied Physics, Atlantic Technological University, Galway, Ireland

ARTICLE INFO

Keywords:
Annular plasmas
Colliding plasmas
Limit of detection
LIBS

ABSTRACT

The purpose of this study is to investigate the possible improvement of the limit of detection of laser induced breakdown spectroscopy using the stagnation layer formed at the centre of an annular plasma. An axicon was used to form an annular plasma on various certified reference targets, the spectra from which were used to construct calibration curves and extract the limit of detection for the system. Comparisons were drawn between the limit of detection for the annular case, dual colliding plasma case and a single plasma case. Clear signal enhancement for certain spectral lines can be seen in the presented spectra. The limits of detection between systems are similar, but the stagnation layer produced from an annular plasma produces the lowest value, for the lowest laser power density and hence least target damage. The signal enhancement and improved limit of detection, at lower power densities, from a stagnation layer at the centre of an annular plasma is a promising result.

1. Introduction

Laser induced breakdown spectroscopy (LIBS) is a well-developed analytical technique which requires no sample preparation and promises fast, minimally destructive, qualitative and quantitative sample analysis. A significant body of work has been carried out towards the lowering of the limit of detection (LOD) of LIBS for many different elements in a whole host of matrices. This work includes investigations into the effects of; laser fluence, wavelength and pulse length as well as space and time optimization along with double pulse arrangements [1–4]. Limits of detection have gradually dropped over the years so that values in the parts per million are possible with LIBS in the UV–visible range of the spectrum. [5–10] while values down to 1 ppm have been achieved with vacuum-UV LIBS, e.g., for the detection of carbon in steel [11–13]. In this contribution the focus is on UV–Visible LIBS, albeit the target is held in vacuum so that the annular plasma can expand to form a region of stagnated plasma (often referred to as a stagnation layer) along its axis of symmetry, normal to the target surface.

Traditional stagnation layer generation involves forming two adjacent plasmas, in an ambient gas at a pressure of less than 1×10^{-1} mbar, which expand not just away from the target but also laterally into each other in a direction parallel to the target [14,15]. The plasmas decelerate at the collision plane, with their kinetic energy being converted into excitation energy, forming what is known as a stagnation layer; the two initial plasmas are known as seed plasmas [16]. Most reported studies use a wedge prism to split a beam [17–19] and form two adjacent plasmas. In this work a biprism is used to split the laser beam into two halves for comparison with the annular plasma. We have found that using the Fresnel bi-prism allows us to create two laser spots which are almost identical for the formation of the seed plasmas. This is in contrast to the Wedge prism case where each laser spot has different amounts of astigmatism.

A number of studies have been carried out comparing the dynamics of a laser produced plasma (LPP) produced by both Gaussian and annular laser beams [20–23], but all of these studies were carried out in experimental conditions preventing stagnation layer formation. To the best of our knowledge the only study demonstrating the formation of a stagnation layer within an expanding annular plasma, through time resolved imaging, was carried out by Valenzula-Villaseca et al. [24,25]. Implementation of an annular LPP into a LIBS system has also been reported [26]. But annular LPPs have not been implemented into a low pressure LIBS system. In fact, the effect of beam shape on the

☆ Selected Papers from the 11th International Conference on Laser Induced Breakdown Spectroscopy (20-25 September 2020).

* Corresponding author.
E-mail address: mossy.kelly@gmit.ie (T.J. Kelly).

https://doi.org/10.1016/j.sab.2022.106430
Received 19 January 2022; Received in revised form 19 April 2022; Accepted 20 April 2022
Available online 29 April 2022

performance of LIBS is relatively under-explored even though it has been shown to significantly affect the LIBS performance indicators such as limit of detection [27]. There are also reports of annular plasma generation being effective in studying Thin-Films with LIBS [28].

In this paper we compare a traditional LIBS setup with two modified setups; the first captures emission from a stagnation layer formed between two seed plasmas, while the second captures emission from a stagnation layer formed at the centre of an annular plasma. Given appropriate environmental conditions both of these modified setups will yield a stagnation layer. Acquisition of the line emission from the stagnation layer provides for an evaluation of the performance of these systems for trace element detection in solid aluminium samples. Calibration curves which allow for the determination of the LOD for copper are presented. A comparison of the three setups in terms of signal to background ratio (SBR) and LOD is given. We are not aware of any previous implementations of annular plasmas in a low pressure environment to investigate the viability of the stagnation layer formed as a source for LIBS.

2. Materials and method

Time and space integrated spectroscopy was carried out on four standard aluminium targets containing known concentrations of trace element impurities, copper being the element of interest for the presented results. These spectra were acquired using the setup shown in Fig. 1, at a pressure of 1×10^{-5} mbar. The magnified section of Fig. 1 shows each of the three focussing geometries; namely annular, dual colliding and single plume plasmas. The annular focus was achieved by placing an axicon before the focusing lens, similarly the dual colliding focus was achieved by placing a biprism before the focusing lens. Both the axicon and biprism had a vertex angle of 0.5. For each focusing geometry, fifty single shot acquisitions (exposures) were taken for each target at three different laser energies; 28 mJ, 38 mJ and 52 mJ. These laser energies were set by attenuating a 6 ns pulse from a Nd:YAG laser, the acquisitions were taken using an Andor iStar ICCD with an exposure time of 150 μs, delayed by 130 ns from plasma formation.

A Dove prism was used in line with the collection optics to rotate the image of the plasma by 90 degrees, allowing it to expand along the entrance slit (width set at 60 μm) of the half meter Czerny-Turner spectrometer. The alignment of both stagnation layer types, relative to the slit of the spectrometer is shown in Fig. 2. The focusing of the combined stagnation layer system (seed plasmas plus stagnation layer) was done in a fashion which permitted us to separate the different elements from each other and collect radiation only form the stagnation layer (Fig. 2). In the case of the biprism the seed plasmas are physically separated from the stagnation layer and so they are imaged on either side of the entrance slit preventing them from making any contribution to the observed spectrum. In the case of the annular plasma seed, two actions help to reduce its contribution to negligible. The emission intensity at a time delay of 130 ns from the ring plasma is very weak and also we arrange the imaging to ensure the most of the ring lies below the bottom the entrance slit. For the single plasma plume we aligned its expansion axis with the vertical slit and captured all radiation from the target surface as the plume expanded upwards along the slit.

The irradiances for each focusing geometry and energy combination are given in Table 2. These irradiances were calculated from areas obtained by imaging the craters from 10 shots at 28 mJ for each focusing geometry. These craters are shown in a composite image in Fig. 3, the craters were imaged using a Keyence VHX 5000 optical microscope. The distance between the seed plasmas using the biprism focusing geometry is equal to the outer radius of the annular focusing geometry, at 2.2 mm.

The certified reference materials used for these experiments were supplied by MBH Analytical. Each sample had aluminium as the bulk material and varying amounts of trace elements, with the percentages of Cu and Al listed in Table 1.

3. Theory

3.1. Annular beam generation

Annular beam profiles can be generated from a collimated light source using a variety of techniques; annular apertures [29], tunable acoustic gradient (TAG) lenses [30], spatial light modulators (SLM) [31] and, as used in this study, an axicon [32]. An axicon is a rotationally symmetric prism, which can be either concave or convex [33]. Axicons generate both Bessel and annular beam profiles along the propagation axis. The length of the region along the axis where a Bessel beam forms is known as the depth of focus (DOF) and is defined by Eq. (1), where R is the diameter of the input beam, n is the refractive index of the axicon and α is the vertex angle of the axicon. In practice the beam formed in the area defined by the DOF is a Bessel-Gauss approximation, given the Gaussian input beam [34].

$$DOF = \frac{R}{(n-1)\alpha} \tag{1}$$

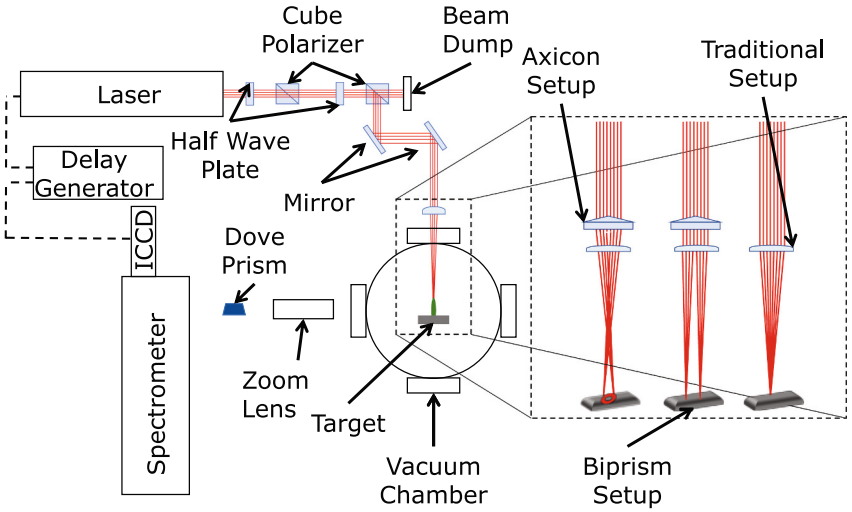

Fig. 1. Experimental setup for time gated spectroscopy of single, dual—colliding and annular plasmas. The laser was a Continuum Surelite III-10 system, the spectrometer a Chromex 0.5 m Czerny-Turner mount and the ICCD was an Andor Technology iSTAR ICCD. A Dove prism was used to rotate the plasma image so that it expanded up along the vertical slit of the stigmatic spectrometer.

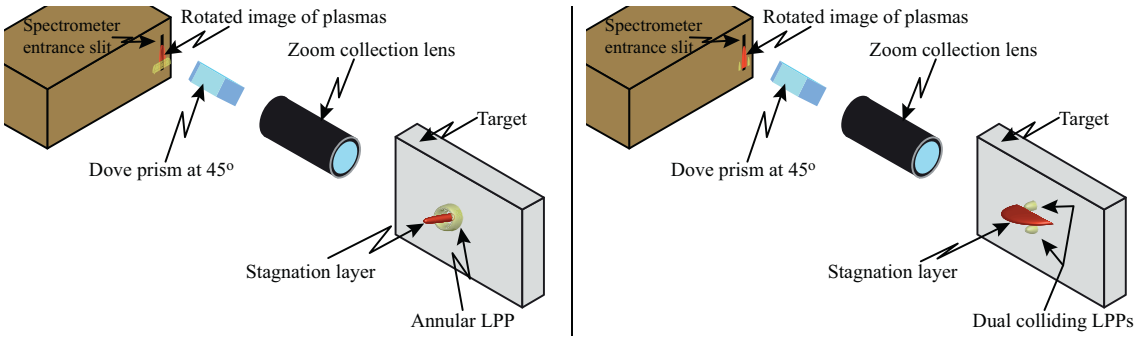

Fig. 2. Schematic of image falling on slit.

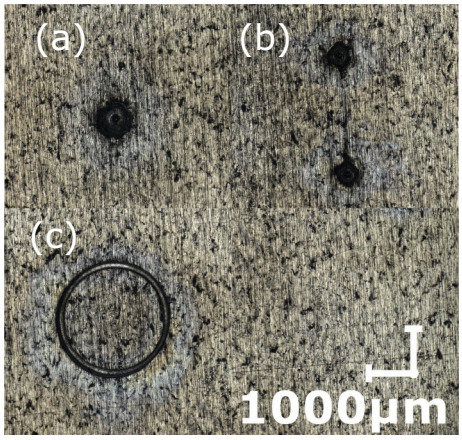

Fig. 3. Crater images for laser produced point, dual and annular plasmas formed on an Al target. The craters represent the accumulation of 10 laser shots.

Table 1
Elemental concentrations of interest contained within the certified reference materials.

Reference Material	Sample Number	Percentage Copper	Percentage Aluminium
XG6082 (B)	1	0.014	97.64
XG6082 (A)	2	0.018	97.71
XG3000B4	3	0.086	96.87
XG6061	4	0.26	97.5

Table 2
Irradiance (W/cm^2) for each focusing geometry.

	28 mJ	38 mJ	52 mJ
Single Plasma	2.3×10^{10}	3.2×10^{10}	4.3×10^{10}
Dual Colliding Plasma	2.1×10^{10}	2.9×10^{10}	3.9×10^{10}
Annular Plasma	3.3×10^{8}	4.5×10^{8}	6.1×10^{8}

Table 3
Signal to background ratios for each focusing geometry and energy combination.

	28 mJ	38 mJ	52 mJ
Single Plasma	5.8	9.2	9.4
Dual Colliding Plasma	4.7	2.8	5.2
Annular Plasma	10.2	6.5	4.2

Table 4
Limit of detection (parts per million) and coefficient of determination for Cu in an Al matrix obtained from the calibration curves constructed for each combination of focusing geometry and laser energy.

Configuration	LOD (ppm)	Line of Best Fit	R^2
Axicon 28 mJ	1.4	$0.976\times + 1502$	0.96
Biprism 28 mJ	18.1	$0.058\times + 268$	0.87
Single 28 mJ	7.8	$0.069\times + 322$	0.84
Axicon 38 mJ	5.4	$0.685\times + 1552$	0.91
Biprism 38 mJ	5.5	$0.222\times + 429$	0.96
Single 38 mJ	1.5	$0.311\times + 360$	0.98
Axicon 52 mJ	6.2	$0.634\times + 2797$	0.99
Biprism 52 mJ	5.7	$0.199\times +1008$	0.83
Single 52 mJ	1.8	$0.510\times + 1395$	0.99

Beyond the DOF an annular beam profile forms, this is the region of interest for this study. The ring-thickness of this annular profile is half the diameter of the beam propagating through the axicon while its outside diameter is given by Eq. (2), where L is the distance from the axicon to the image plane.

$$d_r = 2Ltan[(n-1)\alpha] \tag{2}$$

Through the placement of a lens on the axis of propagation, as shown in Fig. 4, Eq. (2) becomes dependant on f, the focal length of the lens, rather than L, yielding Eq. (3)

$$d_r = 2ftan[(n-1)\alpha] \tag{3}$$

3.2. Limit of detection for LIBS

The limit of detection (LOD) of LIBS is defined as the smallest concentration of a trace element which can be identified from a spectral line. In order for this spectral line to be identifiable it must produce a signal which is greater than three times the standard deviation of the background (counts). The LOD can be expressed using the following equations.

$$X_L = X_B + k.\sigma_B \tag{4}$$

$$X_L - X_B = k.\sigma_B \tag{5}$$

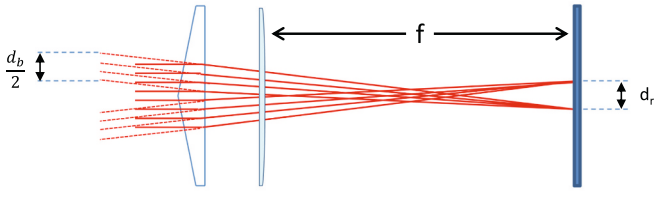

Fig. 4. Schematic diagram showing the formation of an annular focus using the combination of an axicon and a focusing lens. d_b is the laser beam width.

$$LOD = \frac{k.\sigma_B}{S} \quad (6)$$

Where X_L is the lowest discernible response, X_B is the average response due to the background, k is the confidence level within which you are working, in this case 3, σ_B is the standard deviation of the background signal and S is the slope of an intensity versus concentration calibration curve.

4. Results and limit of detection determination

Annular, dual colliding and single plasma spectra were taken for laser pulse energies of 28 mJ, 38 mJ and 52 mJ as shown in Fig. 5. These enabled the determination of signal to background ratios (SBRs) for each case and the construction of calibration curves for each focusing geometry. Signal to background ratios were obtained by dividing the peak intensity of the copper 521.96 nm line by the average signal between 528 nm and 529 nm.

The signal to background ratios for each set of experimental parameters are given in Table 3. These ratios were calculated using the signal captured from target four.

Fig. 6 shows a comparison of the signal, centred at 519 nm, for each target with an input laser energy of 28 mJ. This figure clearly shows a higher level of signal when an annular beam profile is used.

Using the spectra from Fig. 6, the areas under the 521.96 nm Cu neutral peak were used to build the calibration curves presented in Fig. 7. The value for the standard deviation of the background signal was also determined from these plots. In line with the signal to background measurements the standard deviation of the signal between 528 nm and 529 nm, where the spectrum is flat and featureless and thus represents a good measure of the background signal, was taken.

The limit of detection for each combination of experimental parameters is given in Table 4, along with the linear fit parameters and the R^2 value for the fit. The calibration curves show high linearity, but also exhibit large intercept offsets from the expected zero value for zero concentration. Generally, the intercepts associated with the Axicon configuration are higher than the bi-prism and single plasma configurations. We attribute theses offsets to matrix effects which can result in significant non-zero offsets in LIBS calibration curves. The authors of reference [35] have shown that using the laser-assisted LIBS technique which accounts for matrix affects can reduce the offsets.

It is clear from Fig. 5 that, in the case of the axicon configuration, the spectrum is dominated by emission from the neutral species in the plasma whereas for the single, and bi-prism configurations there is more ionic emission. Because we have used the neutral line at 521 nm to determine the limit of detection, the LOD for the axicon case is lower than the other two. The argument is that the laser power density in the axicon case is much lower and so the annular seed plasma will be mainly composed of slower moving neutral species. Hence the resultant stagnation layer will itself have a lower temperature, remembering that kinetic energy of the plasma species converging on the central axis of the annulus is converted into excitation energy and thus to light emission. In summary it appears the axicon case gives the best limit of detection for an energy of 28 mJ which is equal (roughly) to the limit of detection obtained from a single plasma with a laser energy of 38 mJ. Our explanation for these trends broadly follows. In the case of the single plasma plume collisional excitation of neutral species is by binary electron-neutral collisions along with atom-atom and atom-ion collisions involving both trace element and bulk material species. In the case of the bi-prism and annular plasma generation, there is a further contribution to the overall collision rate at the stagnation layer location. In the case of the bi-prism, when the laser energy of the seed plasmas is large this increases the lateral velocity of the plasma plumes and drives a harder stagnation of the colliding seed plasmas resulting in a higher number density of excited emitting species, especially ions over neutrals. This explains why the limit of detection decreases for increasing energy in the bi-prism case. For the annular plasma case the collision of species from the collapsing annular plasma take place along a single axis. At

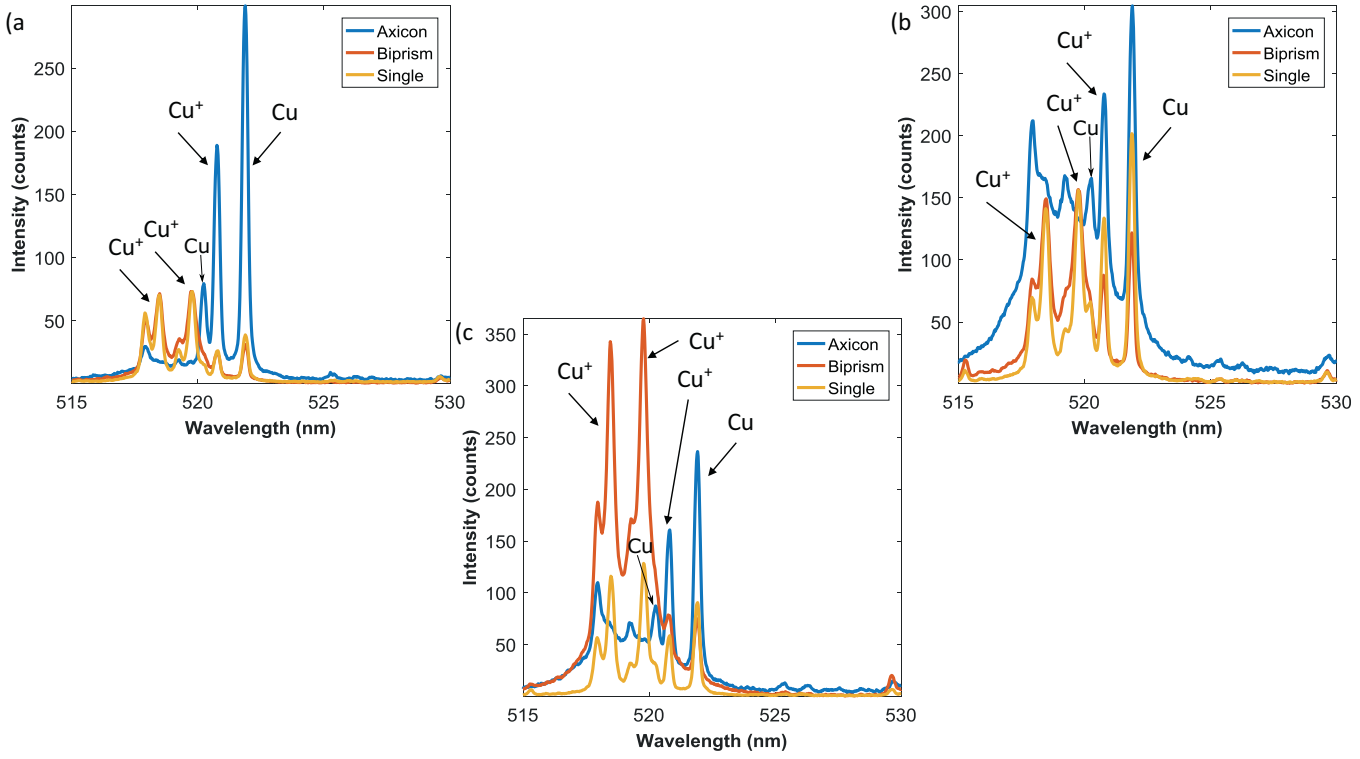

Fig. 5. Time and space integrated spectra centred at 519 nm captured from the stagnation layer formed at the centre of an annular plasma, the stagnation layer formed between two seed plasmas (half of total energy per seed) and a single plasma generated with a laser energy of a) 28 mJ, b) 38 mJ, c) 52 mJ. The target used was number 4 in Table 1 above (0.26% Cu and 97.5% Al).

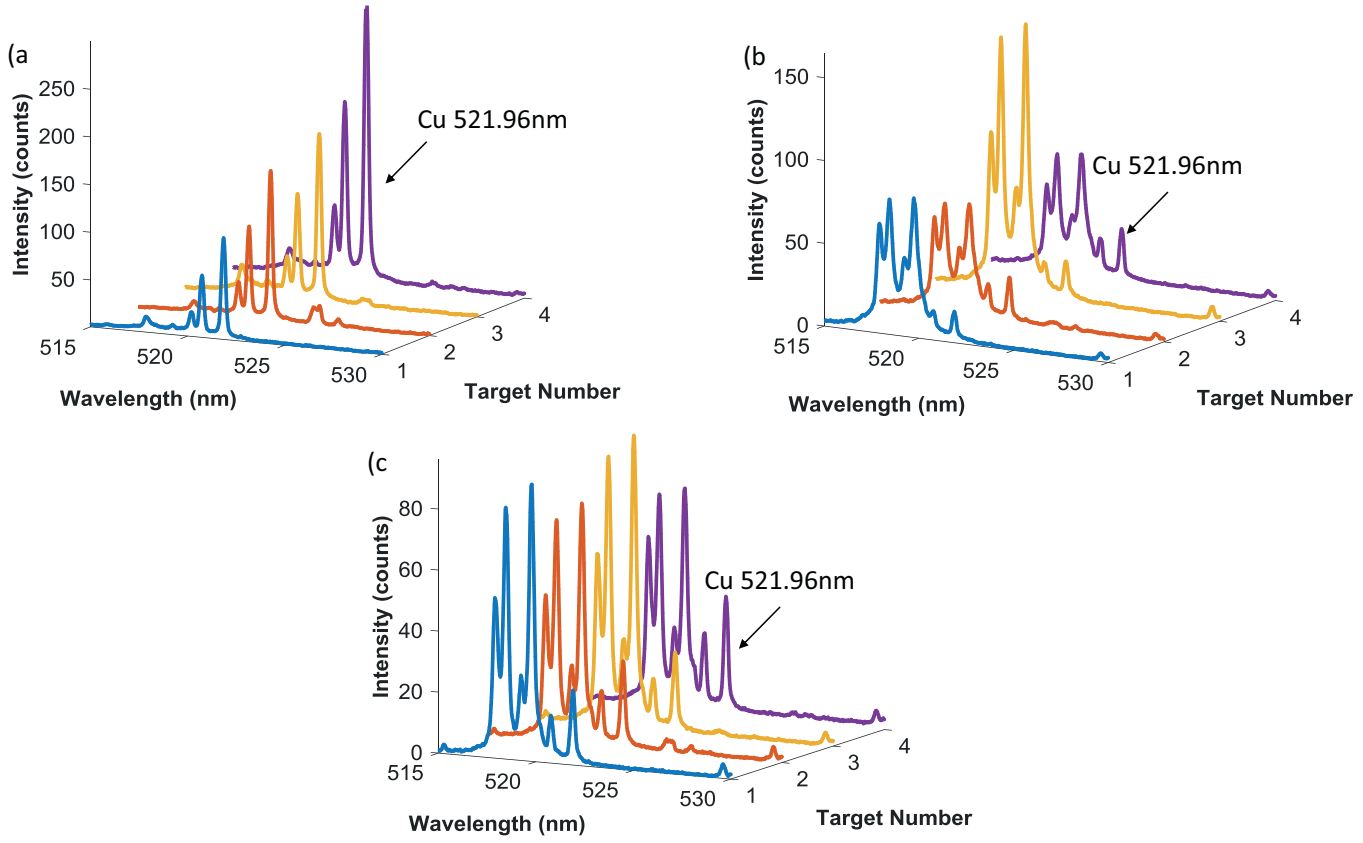

Fig. 6. Time and space integrated spectra centred at 519 nm, for each target, captured from the stagnation layer formed at the centre of a) an annular plasma, b) dual colliding plasma and c) a single plasma generated with a laser energy of 28 mJ.

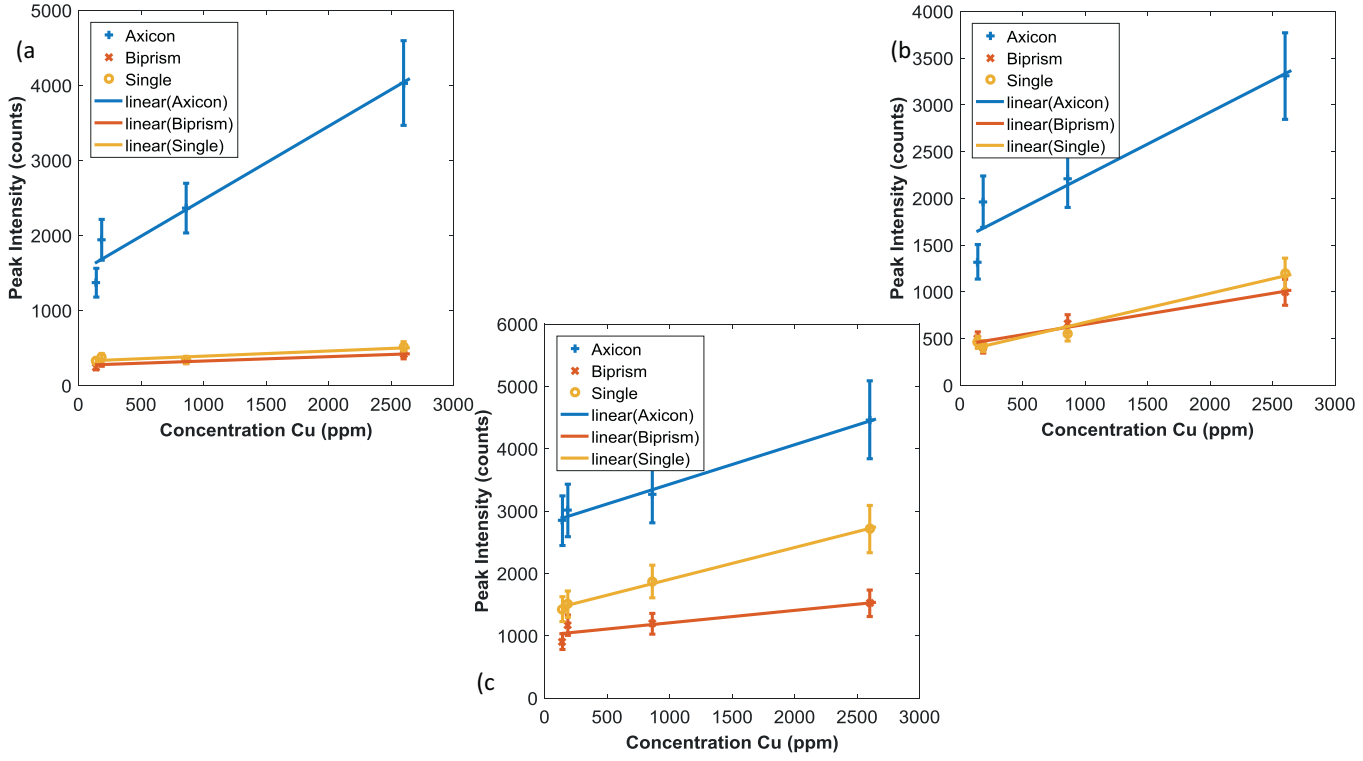

Fig. 7. Calibration curves constructed using the 521.96 nm copper neutral line for each focusing geometry. Plasmas were generated with a laser energy of a) 28 mJ, b) 38 mJ, c) 52 mJ on each of the four targets. A linear regression of each dataset is also shown, the parameters of which are given in Table 4.

lower laser pulse energy (e.g., 28 mJ) this results in mainly neutral species at the stagnation layer. As the laser pulse energy is increased, the proportion of ions increases. This in turn depletes the population of neutrals and is therefore a potential argument as to why the limit of detection is higher at lower laser energies. One piece of evidence to support this assertion is the fact that the relative emission from the ionic species increases for the annular case as the laser energy increases. Ultimately, our data show that the effects induced by the formation of a stagnation layer can significantly alter the emission characteristics and therefore the LIBS performance. Due to the relative ease of its experimental implementation, we can suggest that the stagnation layer can act as an extra control parameter to optimize the performance of a LIBS system.

5. Conclusions

In this work we have presented a novel implementation of stagnation layer formed using annular plasmas into LIBS.

Signal to background ratios and limits-of-detection (LOD) have been presented for the trace element Cu in an Al matrix for three different plasma systems, namely a single plasma plume, a stagnation layer formed in a dual colliding plasma plume experiment and a stagnation layer formed along the axis of symmetry of an annular colliding plasma. Experiments were carried out for three different laser pulse energies, 28 mJ, 38 mJ and 52 mJ, at a pressure of 1×10^{-5} mbar. The neutral copper line at 521.96 nm was chosen for these signal to background ratios and LOD determinations.

For these specific cases the LOD was found to be best for an annular colliding plasma at 28 mJ followed closely by a single plasma plume at 52 mJ, with the full data set for the calibration curves presented in Table 4. While the LOD for both systems is equivalent, with different laser energies, it should be noted that much less material will be ablated with a power density which is two orders of magnitude lower, as is the case for the annular plasma. While the area ablated is larger in the annular case, the damage to the target is less.

The results are promising and warrant further investigation in a wider parameter space, with a particular focus on power density matching between focusing geometries. Such power density matched experiments should make clearer the advantage of annular beam profiles when it comes to LIBS in a low pressure environment.

Declaration of Competing Interest

The authors declare that they have no known competing financial interests or personal relationships that could have appeared to influence the work reported in this paper.

Acknowledgements

BD acknowledges the support of the Irish Research Council through the award of a Government of Ireland Postgraduate Scholarship. Work supported by Science Foundation Ireland Grant Nos. 12/IA/1742 and 19 FFP/6956 along with Sustainable Energy Authority of Ireland (SEAI) Grant No. 19/RDD/556. The work is associated with EU H2020 COST Action No. CA17126 (TUMIEE).

References

[1] D.A. Cremers, L.J. Radziemski, T.R. Loree, Spectrochemical analysis of liquids using the laser spark, Appl. Spectrosc. 38 (5) (1984) 721–729.
[2] D.A. Rusak, B.C. Castle, B.W. Smith, J.D. Winefordner, Fundamentals and applications of laser-induced breakdown spectroscopy, Crit. Rev. Anal. Chem. 27 (4) (1997) 257–290.
[3] O. Samek, D.C.S. Beddows, J. Kaiser, S.V. Kukhlevsky, M. Liska, H.H. Telle, A. J. Whitehouse, Application of laser-induced breakdown spectroscopy to in situ analysis of liquid samples, Opt. Eng. 39 (8) (2000) 2248–2262.
[4] V. Babushok, F. DeLucia, J. Gottfried, C. Munson, A. Miziolek, Double pulse laser ablation and plasma: laser induced breakdown spectroscopy signal enhancement, Spectrochim. Acta B At. Spectrosc. 61 (9) (2006) 999–1014.
[5] D.A. Cremers, R.C. Chinni, Laser-induced breakdown spectroscopy—capabilities and limitations, Appl. Spectrosc. Rev. 44 (6) (2009) 457–506.
[6] D.W. Hahn, N. Omenetto, Laser-induced breakdown spectroscopy (libs), part i: review of basic diagnostics and plasma–particle interactions: still-challenging issues within the analytical plasma community, Appl. Spectrosc. 64 (Dec 2010) 335A–366A.
[7] D.W. Hahn, N. Omenetto, Laser-induced breakdown spectroscopy (libs), part ii: review of instrumental and methodological approaches to material analysis and applications to different fields, Appl. Spectrosc. 66 (Apr 2012) 347–419.
[8] F.J. Fortes, J. Moros, P. Lucena, L.M. Cabalín, J.J. Laserna, Laser-induced breakdown spectroscopy, Anal. Chem. 85 (2) (2013) 640–669 (PMID: 23137185).
[9] J. El Haddad, L. Canioni, B. Bousquet, Good practices in libs analysis: review and advices, Spectrochim. Acta B At. Spectrosc. 101 (2014) 171–182.
[10] L. Jolivet, M. Leprince, S. Moncayo, L. Sorbier, C.-P. Lienemann, V. Motto-Ros, Review of the recent advances and applications of libs-based imaging, Spectrochim. Acta B At. Spectrosc. 151 (2019) 41–53.
[11] J. Jasik, J. Heitz, J.D. Pedarnig, P. Veis, Vacuum ultraviolet laser-induced breakdown spectroscopy analysis of polymers, Spectrochim. Acta B At. Spectrosc. 64 (10) (2009) 1128–1134. A Collection of Papers Presented at the Fifth International Conference on Laser Induced Breakdown Spectroscopy (LIBS 2008).
[12] X. Jiang, P. Hayden, J.T. Costello, E.T. Kennedy, Double-pulse laser induced breakdown spectroscopy with ambient gas in the vacuum ultraviolet: optimization of parameters for detection of carbon and sulfur in steel, Spectrochim. Acta B At. Spectrosc. 101 (jan 2014) 106–113.
[13] F. Trichard, S. Moncayo, D. Devismes, F. Pelascini, J. Maurelli, A. Feugier, C. Sasseville, F. Surma, V. Motto-Ros, Evaluation of a compact vuv spectrometer for elemental imaging by laser-induced breakdown spectroscopy: application to mine core characterization, J. Anal. Atom. Spectr. 32 (2017) 1527–1534.
[14] P.T. Rumsby, J.W.M. Paul, M.M. Masoud, Interactions between two colliding laser produced plasmas, Plasma Phys. 16 (10) (1974) 969.
[15] H. Luna, K.D. Kavanagh, J.T. Costello, Study of a colliding laser-produced plasma by analysis of time- and space-resolved image spectra, J. Appl. Phys. 101 (3) (2007) 33302.
[16] L. Varvarezos, S.J. Davitt, J.T. Costello, T.J. Kelly, The effect of confinement angle on self-colliding aluminium laser plasmas using spectrally resolved fast imaging, Materials 13 (DEC 2020).
[17] P. Hough, C. McLoughlin, S.S. Harilal, J.P. Mosnier, J.T. Costello, Emission characteristics and dynamics of the stagnation layer in colliding laser produced plasmas, J. Appl. Phys. 107 (2) (2010) 24904.
[18] C. Fallon, P. Hayden, N. Walsh, E.T. Kennedy, J.T. Costello, The effect of wedge angle on the evolution of a stagnation layer in a colliding plasma experiment, J. Phys. Conf. Ser. 548 (1) (2014) 12036.
[19] C. Fallon, P. Hayden, N. Walsh, E.T. Kennedy, J.T. Costello, Target geometrical effects on the stagnation layer formed by colliding a pair of laser produced copper plasmas, Phys. Plasma 22 (9) (2015) 93506.
[20] L.M. Cabalín, J.J. Laserna, Atomic emission spectroscopy of laser-induced plasmas generated with an annular-shaped laser beam, J. Anal. Atom. Spectr. 19 (2004) 445–450.
[21] F. Veloso, H. Chuaqui, R. Aliaga-Rossel, M. Favre, I.H. Mitchell, E. Wyndham, Laser-produced annular plasmas, Rev. Sci. Instrum. 77 (6) (2006).
[22] P.N. Malevich, A.N. Chumakov, Improving the efficiency of excitation of ablation plasma spectra with laser irradiation of materials using an axicon/lens system, J. Appl. Spectrosc. 79 (NOV 2012) 838–842.
[23] H.D. Doan, N. Iwatani, H. Sasaki, S. Matsumura, K. Fushinobu, Nanosecond time-resolved visualization of short pulse laser ablation processes for various laser beam profiles, in: Fourteenth Intersociety Conference on Thermal and Thermomechanical Phenomena in Electronic Systems (ITherm), 2014, pp. 1279–1284.
[24] V. Valenzuela-Villaseca, F. Veloso, G. Muñoz-Cordovez, M. Favre, H.M. Ruiz, E. Wyndham, Dynamics of laser produced annular plasmas, J. Phys. Conf. Ser. 1043 (jun 2018) 012046.
[25] V. Valenzuela-Villaseca, R. Hoppe, M. Favre, H. Bhuyan, F. Veloso, E. Wyndham, H. Ruiz, Experiments on laser produced annular plasmas, in: IEEE International Conference on Plasma Science (ICOPS), 2018, pp. 1–1.
[26] R. Hai, L. Sun, D. Wu, Z. He, H. Sattar, J. Liu, W. Tong, C. Li, C. Feng, H. Ding, Enhanced laser-induced breakdown spectroscopy using the combination of circular and annular laser pulses, J. Anal. At. Spectrom. 34 (2019) 1982–1987.
[27] V. Lednev, S.M. Pershin, A.F. Bunkin, Laser beam profile influence on libs analytical capabilities: single vs. multimode beam, J. Anal. Atom. Spectr. 25 (11) (2010) 1745–1757.
[28] E. Surmenko, T. Sokolova, Y.V. Chebotarevsky, I. Popov, Prospects for the libs study of films using an axicon optical system, Laser Phys. 19 (2009) 1373–1376.
[29] J. Durnin, J.J. Miceli, J.H. Eberly, Diffraction-free beams, Phys. Rev. Lett. 58 (Apr 1987) 1499–1501.
[30] A. Mermillod-Blondin, E. McLeod, C.B. Arnold, Dynamic pulsed-beam shaping using a TAG lens in the near UV, Appl. Phys. A 93 (1) (2008) 231.
[31] M. Walde, A. Jost, K. Wicker, R. Heintzmann, Engineering an achromatic bessel beam using a phase-only spatial light modulator and an iterative fourier transformation algorithm, Opt. Commun. 383 (2017) 64–68.
[32] J.H. McLeod, The axicon: a new type of optical element, J. Opt. Soc. Am. 44 (Aug 1954) 592–597.

[33] M. Rioux, R. Tremblay, P.A. Bélanger, Linear, annular, and radial focusing with axicons and applications to laser machining, Appl. Opt. 17 (May 1978) 1532–1536.
[34] F. Gori, G. Guattari, C. Padovani, Bessel-gauss beams, Opt. Commun. 64 (6) (1987) 491–495.
[35] B.C. Windom, D.W. Hahn, Laser ablation-laser induced breakdown spectroscopy (la-libs): a means for overcoming matrix effects leading to improved analyte response, J. Anal. Atom. Spectr. 24 (12) (2009) 1665–1675.